Available online at www.sciencedirect.com

SciVerse ScienceDirect

Procedia Engineering 00 (2015) 000–000

SAND2015-3555C

Procedia Engineering

www.elsevier.com/locate/procedia

The 13th Hypervelocity Impact Symposium

Analysis of impact melt and vapor production in CTH for planetary applications

S. N. Quintana[a,*], D. A. Crawford[b], P. H. Schultz[a]

[a]*Brown University, Department of Earth, Environmental and Planetary Science, 324 Brook Street, Providence, RI 02912, USA*

[b]*Sandia National Laboratories, 1515 Eubank Boulevard Southeast, Albuquerque, NM 87123, USA*

Abstract

This paper explores impact melt and vapor generation for a variety of impact speeds and materials using the shock physics code CTH. The study first compares the results of two common methods of impact melt and vapor generation to demonstrate that both the peak pressure method and final temperature method are appropriate for high-speed impact models (speeds greater than 10 km/s). However, for low-speed impact models (speeds less than 10 km/s), only the final temperature method is consistent with laboratory analyses to yield melting and vaporization. Finally, a constitutive model for material strength is important for low-speed impacts because strength can cause an increase in melting and vaporization.

Keywords: impact melt; impact vaporization; CTH; hydrocode

1. Introduction

The Eulerian shock physics analysis package, CTH, which was developed by Sandia National Laboratories [1,2] is an effective tool for studying a wide variety of high-shock applications. CTH is a two-step Eulerian, finite-difference code that can solve hydrodynamic problems or employ constitutive models in order to simulate material properties such as strength and porosity. The code can perform multi-dimensional, multi-material, strong shock wave physics analyses, and one of its many potential applications is the study of planetary impact cratering. The study of impact cratering often requires accurate melt and vapor representation, which is applicable to Mars [3–6], including impact-vapor related blast winds on Mars [7–9], cometary impacts [10–12], and collisions within the asteroid belt [13–15].

Accurate melt and vapor generation in impact codes is required for thorough and accurate analysis of such planetary impact cratering applications. However, hydrocode models, including CTH, typically do not directly determine phase or entropy information for all equations of state or they do not communicate such information to the end user. Hence, direct melt and vapor determination has been traditionally difficult with shock physics and hydrodynamic codes. Consequently, two methods are often employed to obtain phase information indirectly. The first such method considers the critical pressure required for phase changes to occur. This process has been called the "peak pressure method" [16,17], which will be used in this paper, or the critical entropy method [18]. For the peak pressure method, the critical pressure is calculated from the Hugoniot with the assumption of isentropic release from the shocked state. Phase changes, such as melting or vaporization, are then determined from the peak pressure experienced by the material under shock conditions. The peak pressure method is commonly employed in the planetary science community; studies by Ahrens and O'Keefe [19] and later

* Corresponding author. Tel.: +1-401-863-3594.
E-mail address: stephanie_quintana@brown.edu.

Pierazzo et al. [20], for example, set the standard for using peak shock pressure.

The shock physics community, however, often use the final release-state temperature of the material as a metric for phase changes. The final release state temperature is the temperature of a material once it has been released from the shocked state (after the shockwave has passed). Herein, this method will be referred to as the "final temperature method." In this case, dissipative processes may still add irreversible heating to the system, unlike the peak pressure method, which assumes isentropic release and does not account for such dissipative processes.

The work of Pierazzo et al. [20] focused on the peak pressure method using CSQ, the predecessor to CTH, and inspired follow-on studies for determining the amount of impact-generated melt and vapor. The motivation for this study is that the pressure metric, while robust, cannot address some important impact processes, such as the effect of strength, shear heating by oblique impacts, or the coupled role of temperature in vapor expansion. For example, laboratory experiments indicate that oblique impacts generate significant amounts of vaporization for dolomite and dry ice [21–23]. Hydrocodes using the pressure method, however, were unable to match this observation [24]. Additionally, laboratory shear-friction experiments by van der Bogert et al. [15] documented enhanced melting, even though peak pressure were well below the onset of melting. Hence, a discrepancy appears to exist between theoretical and experimental determination of melt and vapor generation for certain cases, especially in such cases where temperature plays an important role in the impact process. As such, the final temperature method is necessary to understand those processes.

The following analysis also addresses the importance of *strength* in impact processes. Many models are performed hydrodynamically because, for high-speed impacts, peak pressures are attained before the effects of strength become important [25,26]. It is expected, then, that the role of strength is diminished at high speeds, but these results may not be apply to low-speed impacts. We define high-speed above 10 km/s and low-speed below 10 km/s. On the basis of laboratory experiments performed at the NASA Ames Vertical Gun Range [27] in which impact velocities reach a maximum of about 7 km/s, low-speed impacts may induce localized friction-induced melting along fracture zones, even though the peak pressure is extremely low [15]. For oblique impacts, material strength and fracture become even more important as shear melting appears to increase due to friction at fracture zones [15,21,28,29].

The purpose of this study is threefold. First, it verifies the use of the final temperature method as a metric for determining impact melt and vapour generation in CTH for a variety of impact velocities. Second, it demonstrates that the final temperature method is necessary to determine melt (and potentially vaporization) for low-speed impact scenarios. The final objective is to demonstrate that strength plays an important role in the impact generation of both melt and vapor for low-speed impacts. In each case, the models incorporate the semi-analytical equation of state, ANEOS, to describe the thermodynamic properties of each material studied. CTH is capable of using various equations of state, including data tables (such as SESAME); however, we chose to use ANEOS because it is robust and well-defined, materials behave realistically [26], and it has been used extensively in prior work. Furthermore, ANEOS can calculate temperature and pressure simultaneously, and has recently been equipped to communicate phase and entropy to the end user, thereby making it an ideal equation of state for this study.

2. High-Speed Temperature Metric Verification

2.1. Model

In order to verify that the final temperature method for determining melting and vaporization in CTH is appropriate to use in planetary applications, we first develop a high-speed model, based upon the work by Pierazzo et al. [20]. A two-dimensional impact model compares the amount of melt and vapor (combined) produced in an impact for a variety of materials and high impact speeds for both the peak pressure method and final temperature method. For consistency with previous models, the study performed here was completely hydrodynamic; hence, properties such as strength, porosity, and gravity were not included.

The model incorporated a 1 km diameter projectile impacting into a half-space target, which was composed of the same material as the projectile. Impact velocities ranged from 10 to 80 km/s with 10 km/s intervals. Materials tested include aluminum, dunite, granite, iron, and ice. For two-dimensional impacts, a cylindrical domain utilizing axial symmetry necessitates a vertical (90° from horizontal) impact direction. A 90° impact is rare in nature, but the processes observed in such vertical impacts are predominantly characteristic of a larger range of high-angle impacts. Oblique impacts, with angles below 30° from the horizontal, must be treated with three-dimensional models, and are an ongoing part of this study.

In order to attain sufficiently high resolution in the area immediately surrounding the impact point, the verification study incorporated adaptive mesh refinement (AMR), rather than a constant-zoned, flat mesh. AMR allows the use of higher resolution in areas of interest while keeping the rest of the domain at a relatively lower resolution, thus reducing the overall computational cost [30]. The low-speed models attained a resolution of approximately 27 cells per projectile radius around

the impact point, as well as in the melted and vaporized ejecta. The resolution study in Fig. 1 compares results for dunite with an earlier study using 10 cppr, as well as the 20 cppr study by Pierazzo et al. [20]. Some numerical complications can occur with when tracking low degrees of vaporization under vacuum conditions; consequently, an extremely thin CO_2 atmosphere was introduced in order to assist with simulation stability. An atmospheric pressure of 10 Pa was found to have no bearing on the mass of melt and vapor produced during impact.

The "extremum input set" in CTH initializes extra variables to record the maximum or minimum value of a given parameter. This input set was used to record the peak pressure that each cell experienced, and other values of interest such as temperature and entropy were saved as normal cell variables. The mass of material above a certain critical reference value (in this case either peak pressure or temperature required to cause complete melting) was recorded. The masses for material above the critical melting criterion were normalized with the projectile mass and plotted against the melt number for each material. The melt number is defined as U^2/E_m, where U is the impact speed and E_m is the specific energy of melting (the specific energy of the Rankine-Hugoniot state from which isentropic release ends on the liquidus at the 1-bar point [20,31]). Pierazzo et al. [20] use the normalized volume of material, rather than the normalized mass; however, a direct comparison between the two is possible because the conversion factor is simply the reference density.

2.2. Results

To verify the results of the peak pressure model, we compared our results with those of Pierazzo et al. [20] (Fig. 2 (a)). Especially at higher velocities, the two studies agreed well, except for ice. Inconsistencies in the results for ice may stem from differences in the assumed initial temperature for ice. This study assumed an initial temperature of 100 K. If Pierazzo et al. [20] did not change the default initial value for temperature as noted in Barr and Citron [26], the entire domain would be close to melting, which could potentially explain the higher volumes of melted and vaporized ice seen in that study. Stewart and Ahrens [32] performed a detailed experimental shock study of ice, which included two different initial temperatures. A computational study of the sensitivity of the ice equation of state to initial temperature may be performed in the future; however, such a study was not the purpose of this work and will not be included in this contribution. Discrepancies in other materials could originate from difference in model or version of code used. Pierazzo et al. [20] used impactor sizes ranging from 0.2 to 10 km in CSQ, the predecessor of the modern day CTH. Nonetheless, our results from the peak pressure model are in good agreement with the results of Pierazzo et al. [20].

To verify the final temperature method results, we again compared our results with the previous study by Pierazzo et al. [20] (Fig. 2 (b)). As predicted, the results for the temperature method follow the trend evident in the Pierazzo et al. [20] data, which are in good agreement with energy scaling for high velocities (especially with melt numbers above ~30) [33]. The cause of the systematic shifts in the data for different materials is being investigated. Several factors could play a role in the final temperature method results and their offset from the Pierazzo et al. [20] ones. For example, the code and equations of state that this study uses have been updated since the Pierazzo et al. [20] study; thus, some differences in results can be expected. For instance, peak pressures and thus specific energy of melting, calculated from entropy on the Hugoniot differ between the current work and Pierazzo et al. [20] for all materials (Table 1). Additionally, the peak pressure method uses early time pressure for the melt and vapor calculation, while the final temperature method cannot make such calculations until later times when the material has been released from its shocked state. The release from peak pressure is not perfectly isentropic, which is assumed in the peak pressure method. Late time processes and nonisentropic release may account for the offset in final temperature method data and the Pierazzo et al. [20] data and the peak pressure method data from this study (Fig. 2 (c)). Nonetheless, the systematic offset produced by the final temperature method suggests that future studies can use this approach to assess more complex situations.

Table 1. Relevant Pressure and Specific Energy of Melting Comparison

	Basalt		Dunite		Granite		Ice		Aluminum		Iron	
	P97[a]	Current	P97[a]	Current	P97[a]	Current	P97[a]	Current	P97[a]	Current	P97[a]	Current
Complete Melting Pressure (GPa)	116	106	149	170	56	55	3	5	106	101	389	272
Melt Energy x10^6 (J/kg)	9.6	8.7	9.0	10.3	5.2	4.9	0.8	1.2	7.2	6.8	10.0	6.7

[a]Pierazzo et al. [20]

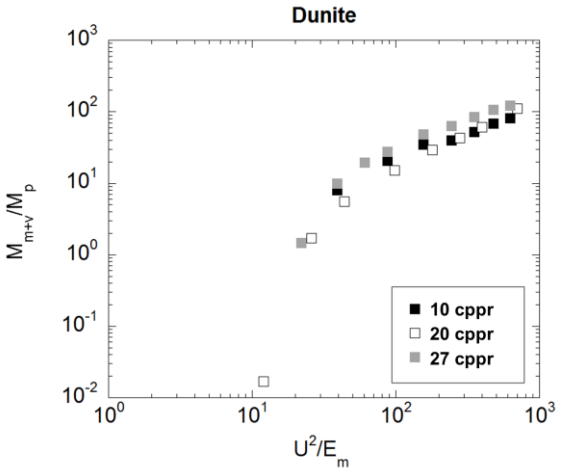

Fig. 1. A resolution study of a hydrodynamic impact of dunite with 10 cells per projectile radius (cppr, black symbols), 20 cppr (open symbols), and 27 cppr, used in this study (gray symbols). Both the 10 and 27 cppr cases used a modern version of CTH, while the 20 cppr case was performed in CSQ by Pierazzo et al.[20]. Differences in the code or library definition of dunite may be responsible for the higher melt mass compared with Pierazzo et al., even in the 10 cppr case.

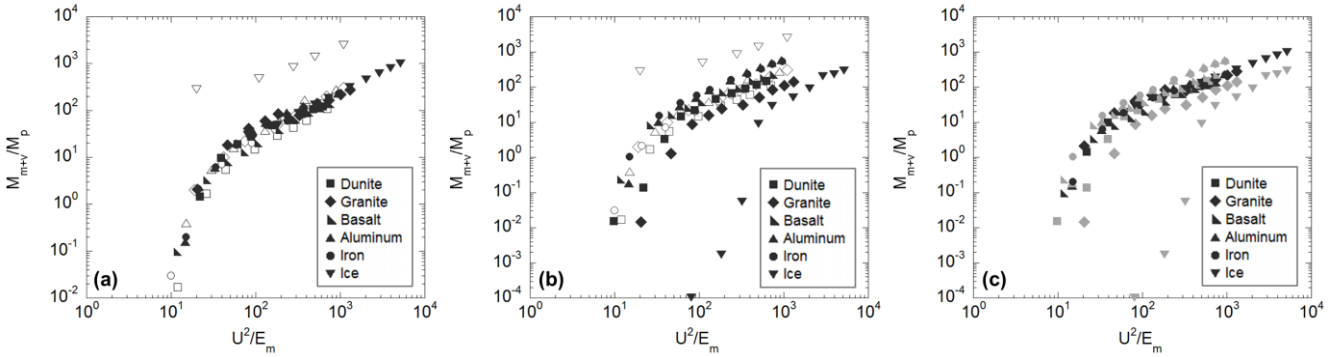

Fig. 2. A comparison of (a) the results of the peak pressure method used in this study (filled symbols) with the results from Pierazzo et al. [20] (open symbols). A similar comparison is shown in (b) for the results of the final temperature method (filled symbols) from this study with the peak pressure method results from Pierazzo et al. [20] (open symbols). (c) is a comparison of results in this study, with the peak pressure method in black symbols and the final temperature method in gray symbols.

3. Low-Speed Impacts

The study detailed above includes only high-speed impacts ranging from 10 to 80 km/s. Such impact velocities are more applicable to collisions on the terrestrial planets, excepting Mars. Lower impact speeds typify impacts within the asteroid belt, early planet formation, and Mars. For such impacts, laboratory experiments provide a particularly useful point of reference. Based upon laboratory shear experiments, van der Bogert et al. [15] argue that even under low peak pressure, localized friction-induced melting can occur along fracture zones. Hypervelocity impact experiments also document significant melt and vapor due to shear heating and re-impacts by the disrupted projectile (for example, Schultz [21] and Schultz et al. [22,23]). Therefore, low-speed impacts also need to be considered.

3.1. Model

The first step in assessing melt and vapor generation at low speeds in a code like CTH is to produce a hydrodynamic two-dimensional model (as noted above). Again, the two-dimensional impacts used axial symmetry and a vertical (90° from horizontal) impact direction for aluminum, basalt, dunite, granite, iron, and ice targets. Basalt was added because it is a geologic material of interest to the planetary community. The simulated impact consisted of a 1 km projectile impacting a planar, half-space target composed of the same material as the projectile at impact speeds spanning 5 to 30 km/s. The most interesting speeds in this case, however, are those less than 10 km/s. High-speed impacts between 10-30 km/s are included in this study for demonstrative and comparative purposes.

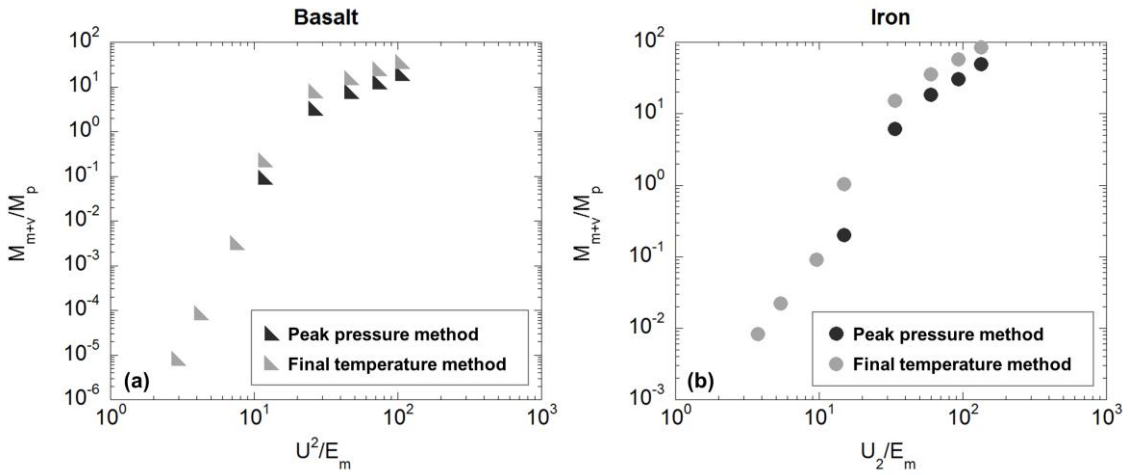

Fig. 3. The results for the peak pressure method (filled symbols) compared with the final temperature method (open symbols) for low speeds for (a) basalt and (b) iron. Only the final temperature method records nonzero values for melt/vapor mass at low velocities.

Unlike the high-speed models discussed above, the low-speed models incorporated adaptive mesh refinement (AMR) in order to attain sufficiently high resolution in the area immediately surrounding the impact point. AMR allows the use of higher resolution in areas of interest while keeping the rest of the domain at a relatively lower resolution, thus reducing the overall computational cost [30]. The low-speed models attained a resolution of approximately 27 cells per projectile radius around the impact point, as well as in the melted and vaporized ejecta. Some complications occur with AMR under vacuum conditions; consequently, an extremely thin CO_2 atmosphere was introduced in order to assist with simulation stability. An atmospheric pressure of 10 Pa was found to have no bearing on the mass of melt and vapor produced during impact.

3.2. Results

As in the high-speed case, masses of material above the critical peak pressure and temperature melting criteria were recorded, then normalized against the projectile mass, and finally plotted against the melt number for each material. As expected, the high-speed results here verified the previous high-speed study using the peak pressure method. At low speeds, however, the peak pressure method did not yield any melting or vaporization for most materials. In fact, only the ice impact generated detectable melt and vapor using the peak pressure criterion for speeds below 8 km/s.

Conversely, the final temperature method yielded small (though non-zero) masses for melt and vaporization at speeds below 8 km/s. At higher speeds, the temperature method results match those of the peak pressure method for most materials. Temperature and peak pressure method results for granite diverge the most (the underlying cause is being investigated). Nevertheless, other materials produce consistent results using the two methods (see the examples of basalt and iron in Fig. 3). In laboratory experiments, even vertical impacts can produce at least some melting and vaporization at speeds near 6 km/s; therefore, the temperature method may indeed be more suited for use at low velocities for melt and vapor determination.

4. Low-Speed Impacts with Strength

Numerical simulations need not be hydrodynamic. Some shock physics codes can incorporate constitutive equations to simulate certain material properties. One-dimensional models provide a verification that CTH and the constitutive models behave as expected, while also providing predictions for the two-dimensional cases. The two-dimensional models allow for direct comparison with the hydrodynamic case detailed in Section 3 above. For geological materials, two separate strength models were tested. One is a geological, pressure-dependent yield surface model. The other geological material strength model is the brittle damage with localized thermal softening (BDL) model developed by Crawford and Schultz [34], which begins with the damage model of Collins et al. [35] and adds crack spacing estimates and shear heating within the cracks, thereby leading to thermal softening [34]. For metals, a linearly elastic, perfectly-plastic model with a von Mises yield surface was used.

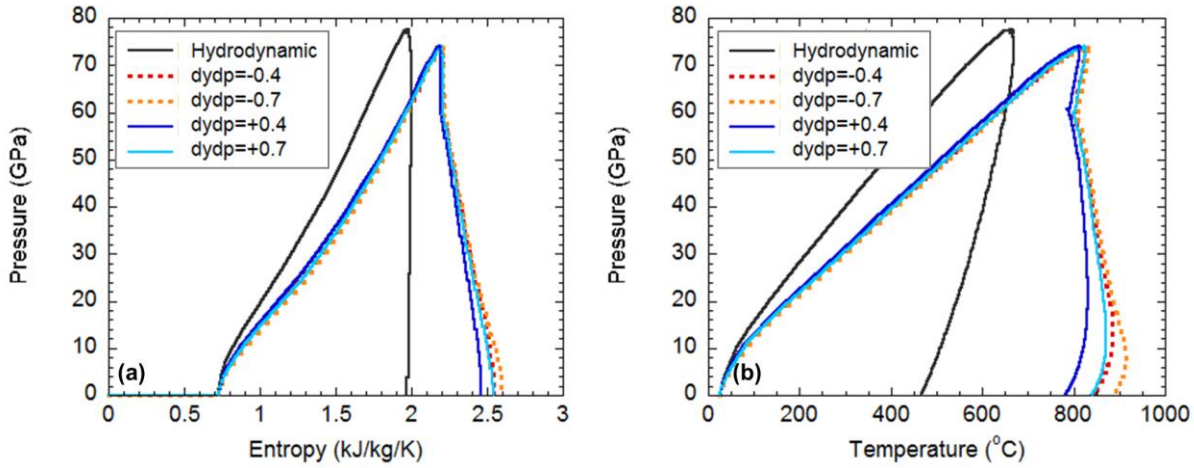

Fig. 4. Some results from the one-dimensional study for a 5 km/s dunite (forsterite) impact using the geological, pressure-dependent yield surface strength model. The solid black line is the hydrodynamic model. The colored lines show the different pressure dependencies on the yield surface, which is what controls the strength of the material. "Dydp" represents the slope of the yield surface. Solid blue lines (positive dydp) represent an unfractured target, while the dotted red lines (negative dydp) represent a fractured target. Pressure vs. entropy is plotted in (a), and pressure vs. temperature is plotted in (b). With the addition of strength, peak pressure decreases from the hydrodynamic case, entropy increases, and final release-state temperature increases. A fractured target (more negative dydp) generates more melt than an unfractured target (positive dydp).

4.1. One-dimensional model and results

The initial simulation simply used a one-dimensional impact of a flyer plate into a target composed of the same material at speeds between 5 and 30 km/s for targets of aluminum, basalt, dunite, granite, water ice, and iron. For the one-dimensional models, a high-resolution (125 cells per projectile length) flat mesh was used. A set of hydrodynamic models was run first for comparison, followed by a set of models incorporating strength. The one-dimensional study employed the pressure-depended yield surface strength model (with both fractured and non-fractured target material) and the von Mises yield surface strength model, but did not include the BDL strength model.

Plots of pressure vs. entropy and pressure vs. temperature for the strength case coincide with the hydrodynamic case at high speeds, meaning that strength did not have a significant effect. When strength (especially the pressure-dependent yield surface model) was included at low speeds, however, three effects emerged (Fig. 4): the peak pressure of the system decreased, the final entropy of the system increased, and the final release-state temperature of the system increased. An increase in entropy and final release-state temperature in the one-dimensional models suggests that strength may cause an increase in melting compared to what would be expected from a hydrodynamic calculation in the two-dimensional models at low speeds. Additionally, the fact that peak pressure decreased but final release-state temperature actually increased in the one-dimensional strength model runs suggests that the peak pressure method may yield less melt mass at low speeds than the final temperature method in the two-dimensional models.

4.2. Two-dimensional model and results

The two-dimensional case allowed for direct comparison of melt and vapor generation between a hydrodynamic target and one with strength. The model from Section 3 (above) was changed in order to include an appropriate strength model, depending on the material. All other factors besides strength are the same as the model in Section 3. For geologic materials (dunite, basalt, granite, and ice), the pressure-dependent yield surface model incorporated a slightly fractured to highly fractured target prior to impact. Such a weakened target would be expected in nature, as rocks do not behave as solid slabs at scales of tens of kilometers. The highly fractured target provided an upper bound for the expected amount of melt. In theory, highly fractured material can produce large amounts of irreversible target heating, which can lead to increased melting, similar to porous materials (for example, Zel'dovich and Raizer [36] and Wünnemann et al. [37]), though porosity was not included here. Moreover, the BDL strength model was also tested for dunite, basalt, and granite, because these materials have been characterized by Crawford and Schultz [34]. Strength for aluminum and iron was provided by the von Mises yield surface model.

As expected from the one-dimensional models, the mass of melt and vapor produced in the high-speed verification check models is nearly equivalent to the mass of melt and vapor produced in the hydrodynamic case (see the examples for basalt

and dunite in Fig. 5). Thus, strength does not significantly affect melt and vapor production at high speeds for vertical impacts. The effect of strength during oblique impacts is forthcoming.

For low-speed impacts, though, strength appears to have the general effect predicted from the one-dimensional models predominantly for basalt (Fig. 5 (a)), dunite (Fig. 5 (b)), and granite: the inclusion of a strength yields more melting and vaporization. It is more difficult in the two-dimensional case to determine whether the highly fractured target produced more melting and vaporization than the moderately fractured target, likely due to the complexity of the two-dimensional model compared to the one-dimensional model. In general, this study demonstrates that strength may be an important factor to consider and should not be ignored for low-speed impacts. If a hydrodynamic model only is used, the amount of melting produced may be underestimated.

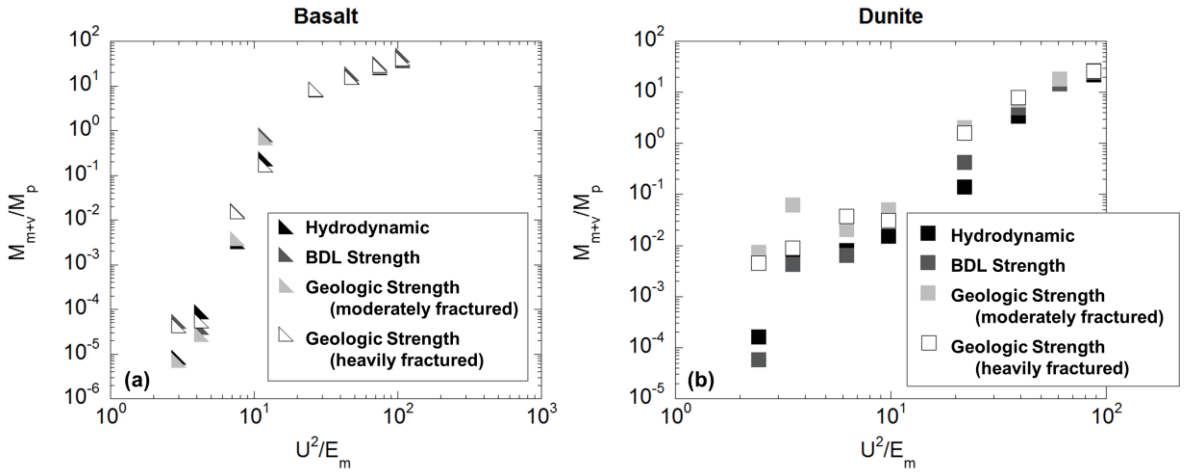

Fig. 5. Results from the low-speed strength study using the final temperature method for (a) basalt and (b) dunite. At high speeds for both materials, strength appears to have a negligible effect on melt and vapor formation compared with the hydrodynamic case. However, both the pressure-dependent yield surface model (denoted "Geologic strength" model in the figure) and the BDL strength model generate deviations in the amount of melt and vapor generated at lower speeds.

5. Summary

In summary, this study produced three major results. First, it demonstrated the validity of the final temperature method as a metric for determining melt and vapor generation. The cause of the offset in the final temperature data is being investigated, yet the systematic offset indicates that this approach may be still be used in the same applications as the peak pressure method. Temperature is important, and even necessary, to more completely understand the impact process in some cases. Second, the final temperature method reveals melt and vapor generation, even at low impact speeds, consistent with laboratory studies. Melt and vapor generation is expected to increase for oblique impacts, as demonstrated in the laboratory, but such studies must be performed with three-dimensional models. A three-dimensional analysis for low-speed impacts incorporating material strength is forthcoming. Finally, for vertical impacts at impact high speeds, models with strength behave in the same manner as the hydrodynamic models, thereby indicating that strength has little effect on melt and vapor generation at such high speeds, at least for vertical impacts. Conversely, material strength has a notable effect on melt and vapor generation at low impact speeds, and the temperature method, rather than the peak pressure method, is appropriate for melt and vapor analysis in such conditions.

Acknowledgements

Sandia is a multiprogram laboratory operated by Sandia Corporation, a Lockheed Martin Company, for the United States Department of Energy under Contract DE-AC04-94AL85000. Part of this work was performed under the NASA Mars Fundamental Research Program (MFRP) grant NNX13AG43G. The material herein is also based upon work partially supported by the National Science Foundation Graduate Research Fellowship under grant number DGE-1058262. Any opinion, findings, and conclusions or recommendations expressed in this material are those of the authors and do not necessarily reflect the views of the National Science Foundation or Sandia National Laboratories.

References

[1] McGlaun, J.M., Thompson, S.L., Elrick, M.G., 1990. CTH: A three-dimensional shock wave physics code, International Journal of Impact Engineering 10, pp. 351–360.
[2] Hertel, Jr, E.S., Bell, R.L., Elrick, M.G., Farnsworth, A.V., Kerley, G.I., et al., 1993. "CTH: A Software Family for Multi-Dimensional Shock Physics Analysis," Proceedings of the 19th International Symposium on Shock Waves, pp. 377–382.
[3] Clifford, S.M., Cintala, M.J., Barlow, N.G., 1991. An Estimate of the Global Thickness of Impact Melt on Mars, Lunar and Planetary Institute Science Conference, Universities Space Research Association. Houston, TX, paper #223.
[4] Schultz, P.H., Mustard, J.F., 2004. Impact melts and glasses on Mars, Journal of Geophysical Research: Planets. 109.
[5] Johnson, J.R., Staid, M.I., Titus, T.N., Becker, K., 2006. Shocked plagioclase signatures in Thermal Emission Spectrometer data of Mars, Icarus 180, pp. 60–74.
[6] Wrobel, K.E., Schultz, P.H., 2004. Effect of planetary rotation on distal tektite deposition on Mars, Journal of Geophysical Research 109.
[7] Schultz, P.H., Quintana, S.N., 2012. Impact blast winds: Origin of certain permanent wind streaks on Mars, Geological Society of America 2012 Annual Meeting, Geological Society of America. Charlotte, NC, p. 534.
[8] Schultz, P.H., Quintana, S., 2013. Impact Blast Wind Scouring on Mars, Lunar and Planetary Institute Science Conference, Universities Space Research Association. Houston, TX, paper #2697.
[9] Quintana, S.N., Schultz, P.H., 2013. Modeling impact blast winds on Mars: The formation of permanent wind streaks, Geological Society of America 2013 Annual Meeting, Geological Society of America. Denver, CO, p. 486.
[10] Gibson, E.K., Moore, G.W., 1973. Volatile-Rich Lunar Soil: Evidence of Possible Cometary Impact, Science 179, pp. 69–71.
[11] Schultz, P.H., Gault, D.E., 1990. Prolonged global catastrophes from oblique impacts, Geological Society of America Special Papers 247, pp. 239–262.
[12] Bruck Syal, M., Schultz, P.H., Crawford, D.A., 2013. Cometary Coma Collisions on the Moon, Lunar and Planetary Institute Science Conference, Universities Space Research Association. Houston, TX, paper #2569.
[13] Keil, K., Stoeffler, D., Love, S.G., Scott, E.R.D., 1997. Constraints on the role of impact heating and melting in asteroids, Meteoritics & Planetary Science 32, pp. 349–363.
[14] Davison, T.M., Ciesla, F.J., Collins, G.S., 2012. Post-impact thermal evolution of porous planetesimals, Geochimica et Cosmochimica Acta 95, pp. 252–269.
[15] Van Der Bogert, C.H., Schultz, P.H., Spray, J.G., 2003. Impact-induced frictional melting in ordinary chondrites: A mechanism for deformation, darkening, and vein formation, Meteoritics & Planetary Science 38, pp. 1521–1531.
[16] Quintana, S.N., Crawford, D.A., Schultz, P.H., 2012. Verification of Impact Melt and Vapor Determination Methods in CTH, Geological Society of America 2012 Annual Meeting, Geological Society of America. Charlotte, NC, p. 482.
[17] Quintana, S.N., Crawford, D.A., Schultz, P.H., 2013. Verification of Impact Melt and Vapor Determination Methods in CTH, Lunar and Planetary Institute Science Conference, Universities Space Research Association. Houston, TX, paper #1733.
[18] Kraus, R.G., Senft, L.E., Stewart, S.T., 2011. Impacts onto H2O ice: Scaling laws for melting, vaporization, excavation, and final crater size, Icarus 214, pp. 724–738.
[19] Ahrens, T.J., O'Keefe, J.D., 1972. Shock melting and vaporization of lunar rocks and minerals, Earth, Moon and Planets 4, pp. 214–249.
[20] Pierazzo, E., Vickery, A.M., Melosh, H.J., 1997. A Reevaluation of Impact Melt Production, Icarus 127, pp. 408–423.
[21] Schultz, P.H., 1996. Effect of impact angle on vaporization, Journal of Geophysical Research 101, pp. 21117–21136.
[22] Schultz, P.H., Sugita, S., Eberhardy, C.A., Ernst, C.M., 2006. The role of ricochet impacts on impact vaporization, International Journal of Impact Engineering 33, pp. 771–780.
[23] Schultz, P.H., Eberhardy, C.A., Ernst, C.M., A'Hearn, M.F., Sunshine, J.M., Lisse, C.M., 2007. The Deep Impact oblique impact cratering experiment, Icarus 191, pp. 84–122.
[24] Pierazzo, E., Kring, D.A., Melosh, H.J., 1998. Hydrocode simulation of the Chicxulub impact event and the production of climatically active gases, Journal of Geophysical Research: Planets 103, pp. 28607–28625.
[25] Melosh, H.J., 1989. Impact Cratering: A Geologic Process, Oxford University Press, New York.
[26] Barr, A.C., Citron, R.I., 2011. Scaling of melt production in hypervelocity impacts from high-resolution numerical simulations, Icarus 211, pp. 913–916.
[27] Gault, D.E., Wedekind, J.A., 1978. "Experimental studies of oblique impact," Lunar and Planetary Science Conference Proceedings 9, pp. 3843–3875.
[28] Spray, J.G., 1998. Localized shock- and friction-induced melting in response to hypervelocity impact, Geological Society, London, Special Publications 140, pp. 195–204.
[29] Senft, L.E., Stewart, S.T., 2009. Dynamic fault weakening and the formation of large impact craters, Earth and Planetary Science Letters 287, pp. 471–482.
[30] Crawford, D. A., 1999. Adaptive Mesh Refinement in CTH, Technical Report #SAND99-1118C, Sandia National Laboratories, May 1999.
[31] Bjorkman, M.D., Holsapple, K.A., 1987. Velocity scaling impact melt volume, International Journal of Impact Engineering 5, pp. 155–163.
[32] Stewart, S.T., Ahrens, T.J., 2005. Shock properties of H2O ice, Journal of Geophysical Research 110.
[33] O'Keefe, J.D., Ahrens, T.J., 1977. Impact-induced energy partitioning, melting, and vaporization on terrestrial planets, Lunar and Planetary Institute Science Conference Proceedings 8, pp. 3357–3374.
[34] Crawford, D.A., Schultz, P.H., 2013. A model of localized shear heating with implications for the morphology and paleomagnetism of complex craters, Large Meteorite Impacts and Planetary Evolution 5. Sudbury, Canada, paper #3047.
[35] Collins, G.S., Melosh, H.J., Ivanov, B.A., 2004. Modeling damage and deformation in impact simulations, Meteoritics & Planetary Science 39, pp. 217–231.
[36] Zel'dovich, Y.B., Raizer, Y.P., 1966. Physics of Shock Waves and High-Temperature Hydrodynamic Phenomena, New York, pp. 269–276.
[37] Wünnemann, K., Collins, G.S., Osinski, G.R., 2008. Numerical modelling of impact melt production in porous rocks, Earth and Planetary Science Letters 269, pp. 530–539.